Brooks and Wallingford, http://www.jcb.org/cgi/content/full/jcb.201204072/DC1

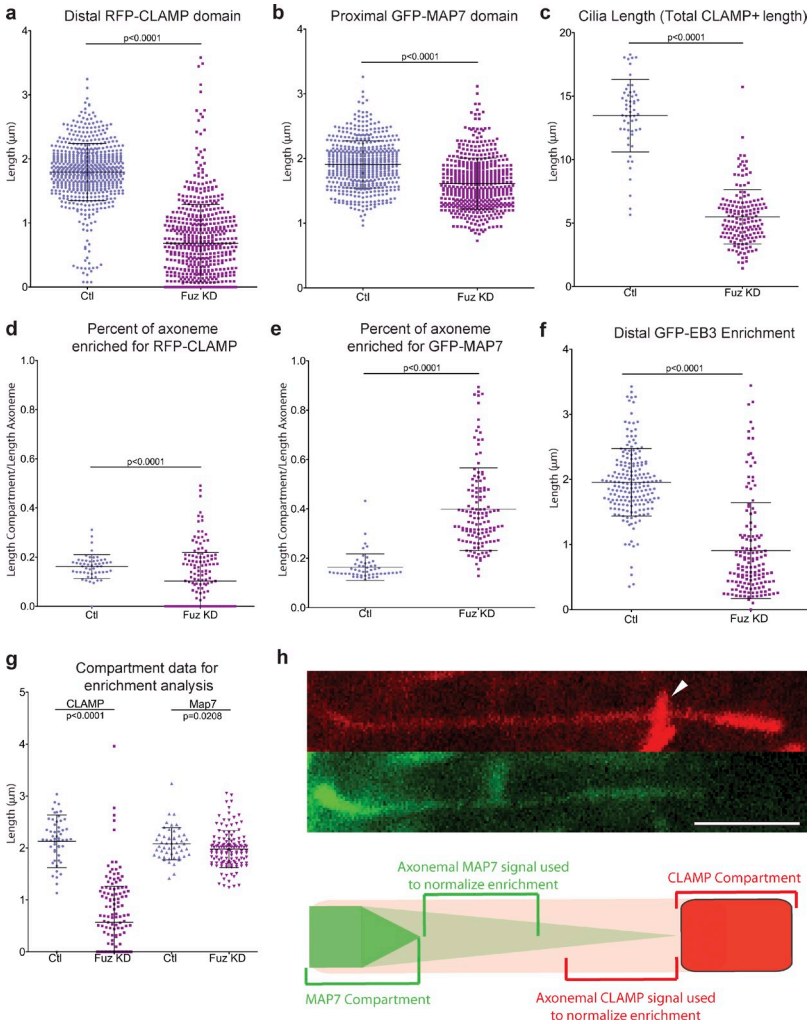

Figure S1. **Quantification of ciliary compartments in control and Fuz KD axonemes.** (a) Graph of distal RFP-CLAMP compartment length of control (Ctl) and Fuz KD cells. RFP-CLAMP compartment length is severely reduced in Fuz KD cells, as compared with controls (Fuz KD [mean ± SD = 0.68 ± 0.61; *n* = 652] vs. control [1.80 ± 0.45; *n* = 582; P < 0.0001]). (b) Graph of proximal GFP-MAP7 compartment length. GFP-MAP7 compartment length is only modestly reduced in Fuz KD cells, as compared with controls (Fuz KD [mean ± SD = 1.61 ± 0.39; *n* = 523] vs. control [1.91 ± 0.36; *n* = 516; P < 0.0001]). (c) Total ciliary length (as measured by RFP-CLAMP) is reduced in Fuz KD axonemes, as compared with controls (Fuz KD [mean ± SD = 5.49 ± 2.14; *n* = 54] vs. control [13.46 ± 2.87; *n* = 161; P < 0.0001]). (d) The percentage of the axoneme occupied by the enriched CLAMP compartment is decreased upon Fuz KD (37% reduction; Fuz KD [mean ± SD = 0.10 ± 0.12; *n* = 161] vs. control [0.16 ± 0.05; *n* = 54; P < 0.0001]). (e) The percentage of the axoneme occupied by the enriched MAP7 domain is increased upon Fuz KD (59% increase; Fuz KD [mean ± SD = 0.40 ± 0.18; *n* = 130] vs. control [0.16 ± 0.05; *n* = 52; P < 0.0001]). Note that this increase is not caused by a lengthening of the MAP7 compartment in absolute terms (see g). (f) EB3, another marker of the distal compartment, is also severely reduced (54% mean reduction; Fuz KD [mean ± SD = 0.91 ± 0.74; *n* = 146] vs. control [1.96 ± 0.52; *n* = 189; P < 0.0001]). (g) A plot of the compartment lengths of the subset of CLAMP and MAP7 data in which it was possible to also measure the full length of the axoneme (by RFP-CLAMP). These data were used to calculate the percentage of axoneme length occupied by the compartments. We were unable to accurately measure the full length of short axonemes in control cells, as their signal was lost in the ciliary tuft. Therefore, the mean length of the CLAMP domain is slightly elevated in this dataset, as compared with the whole dataset presented in a. Additionally, this dataset slightly underreports the difference in MAP7 length between control and Fuz KD conditions when compared with the dataset in b. (h, top) Localization of RFP-CLAMP and GFP-MAP7 in a single axoneme. Note that each marker is highly enriched in a subset of the axoneme but that both markers are also found at low levels outside of these enriched areas. The white arrowhead in the CLAMP image indicates the tips of other cilia overlying the axoneme (note that in this case, the intensity was measured proximal to these tips). Bars, 3 µm. (bottom) A schematic of this localization describing how enrichment of the compartments was calculated.

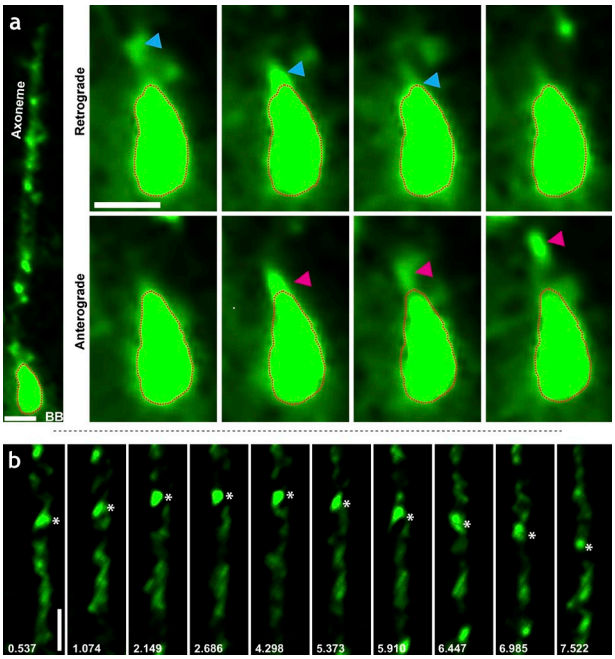

Figure S2. **GFP-IFT20 behavior at the base and tips of axonemes.** (a, left) Still frame from a high-speed confocal video of a single axoneme from a GFP-IFT20–expressing cell. The red outline indicates peri-basal body (BB) IFT signal. (top right) Still frames from a high-speed time-lapse video showing the transition of a retrograde particle of GFP-IFT20 (blue arrowheads) from the axoneme into the basal body IFT pool (red outlines). (bottom right) Still frames from the same video showing the entry of an anterograde GFP-IFT20 particle (pink arrowheads) into the axoneme from the basal body (red outlines). Also see Video 4. (b) Still frames from a time-lapse video showing a GFP-IFT20–labeled particle moving anterograde, pausing, and beginning to move in a retrograde fashion. Distal is up in the figure; note that additional GFP-IFT20 signal is present distal to the point of reversal. Asterisks indicate a single pausing IFT train. Note the presence of other IFT trains distal to the pausing train. Bars, 1 µm.

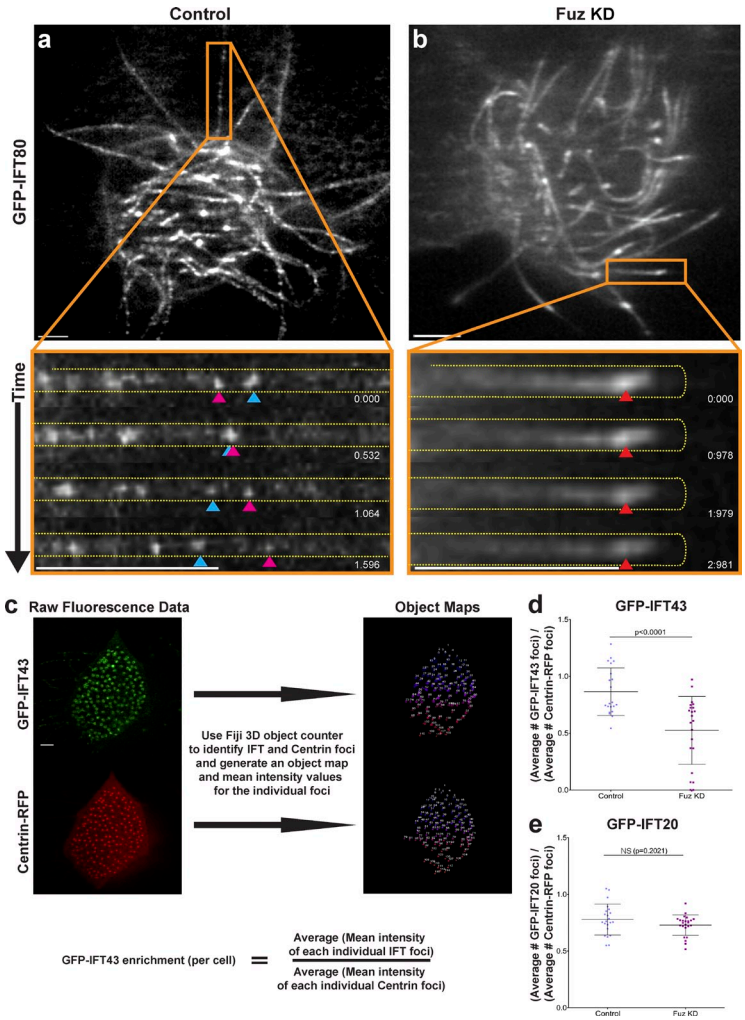

Figure S3. **Fuzzy is required for IFT80 dynamics in the axoneme and for localization of IFT43 to peri-basal body pools.** (a) Still frame from a confocal video showing a GFP-IFT80 in a control multiciliated cell (Video 7). The orange box represents the region shown in the bottom image, which depicts successive still frames from a time-lapse video showing the processive movement of GFP-IFT80–labeled particles. Time is indicated in seconds. Pink arrowheads indicate anterograde particles; blue arrowheads indicate retrograde particles. (b) Still frame from a high-speed confocal video of GFP-IFT80 in a Fuz KD cell (Video 8). The orange box represents the region shown in the bottom image, which depicts still frames from a time-lapse video revealing abnormally large and immotile IFT80-labeled particles (red arrowheads). (a and b) The axoneme is outlined in yellow. (c) Schematic explanation of quantification methodology used for assessing enrichment of GFP-IFT43 at the apically localized basal bodies. To quantitate GFP-IFT43 recruitment, we used an object detection algorithm to identify foci of GFP-IFT43 and Centrin-RFP. We then averaged together the mean intensities of all detected GFP-IFT43 foci in a single cell and normalized it to the averaged mean intensities of all Centrin-RFP foci. Bar, 3 µm. (d) Quantification of the number of GFP-IFT43 foci detected per Centrin-RFP foci per cell. Fuz KD led to a significant reduction in this value (Fuz KD [mean ± SD = 0.52 ± 0.30; *n* = 22 cells; six embryos] vs. control [0.86 ± 0.21; *n* = 21 cells; six embryos; P < 0.0001]). (e) There is no significant difference in the number of GFP-IFT20 foci per Centrin-RFP foci in control versus KD conditions (Fuz KD [mean ± SD = 0.73 ± 0.09; *n* = 24 cells; six embryos] vs. control [0.78 ± 0.14; *n* = 22 cells; six embryos, P = 0.2021]).

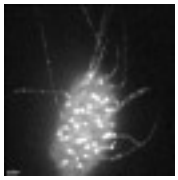

Video 1. **Dynamics of GFP-IFT20 in a control multiciliated cell.** A single control multiciliated cell is shown. Time-lapse images were acquired at 500-ms intervals for a total of 11.477 s by high-speed confocal microscopy on a microscope (LSM 5 LIVE). The video is played back at 4 frames/s. Also see Fig. 2.

Video 2. **High-magnification view of GFP-IFT20 dynamics in a control axoneme.** A single axoneme from Video 1 is shown. GFP-IFT20 particles move both antero- and retrogradely. The axoneme is outlined in yellow; distal is to the right. Time-lapse images were acquired at 500-ms intervals for a total of 11.477 s by high-speed confocal microscopy on a microscope (LSM 5 LIVE). The video is played back at 6 frames/s. See Fig. 2.

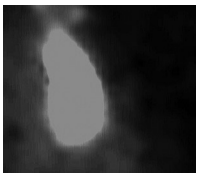

Video 3. **Dynamics of GFP-IFT20 at the basal body–axoneme junction.** As the video starts, a retrograde particle can be seen entering the peri-basal body IFT pool from the axoneme. Immediately thereafter, an anterograde particle can be seen entering the axoneme. Additional similar events can be observed throughout the video. Time-lapse images were acquired at 500-ms intervals for a total of 50 s by high-speed confocal microscopy on a microscope (LSM 5 LIVE). The video is played back at 12 frames/s. See Fig. S2.

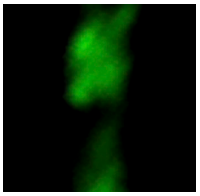

Video 4. **Reversal of GFP-IFT20–labeled IFT trains.** Note the presence of additional GFP-IFT20 trains distal to (above) the point of reversal. The arrowhead indicates a pausing IFT train, with other IFT trains visible distal to the pausing event. Time-lapse images were acquired at 500-ms intervals for a total of 42 s by high-speed confocal microscopy on a microscope (LSM 5 LIVE). The video is played back at 12 frames/s. Also see Fig. S2.

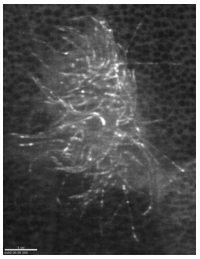

Video 5. **Large, immotile GFP-IFT20 aggregations in a Fuz KD multiciliated cell.** A single multiciliated cell from a Fuz KD embryo is shown. Visible GFP-IFT20 particles are static for the entire length of the video. Time-lapse images were acquired at 561-ms intervals for a total of 10.674 s by high-speed confocal microscopy on a microscope (LSM 5 LIVE). The video is played back at 6 frames/s. For more information, see Fig. 3.

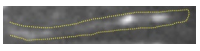

Video 6. **High-magnification view of static GFP-IFT20 aggregations in a Fuz KD axoneme.** A single axoneme from Video 5 is shown. The axoneme is outlined in yellow; distal is to the right. Time-lapse images were acquired at 561-ms intervals for a total of 10.674 s by high-speed confocal microscopy on a microscope (LSM 5 LIVE). The video is played back at 6 frames/s. See Fig. 3.

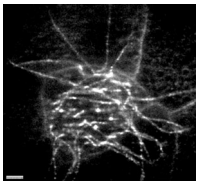

Video 7. **Dynamics of GFP-IFT80 in a control multiciliated cell.** A single control multiciliated cell is shown. Time-lapse images were acquired at 532-ms intervals for a total of 6.916 s by high-speed confocal microscopy on a microscope (LSM 5 LIVE). The video is played back at 6 frames/s. See Fig. S3. Bar, 3 µm.

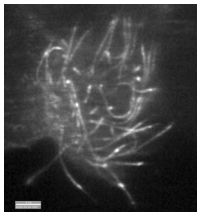

Video 8. **Fuz KD leads to large, immotile GFP-IFT80 aggregations.** A single multiciliated cell from a Fuz KD embryo is shown. Visible GFP-IFT80 particles are static for the length of the video. Time-lapse images were acquired at 500-ms intervals for a total of 6.488 s by high-speed confocal microscopy on a microscope (LSM 5 LIVE). The video is played back at 6 frames/s. See Fig. S3.

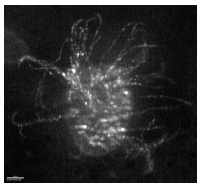

Video 9. **Dynamics of GFP-IFT43 in a control multiciliated cell.** A single control multiciliated cell expressing GFP-IFT43 is shown. Time-lapse images were acquired at 536-ms intervals for a total of 16.100 s by high-speed confocal microscopy on a microscope (LSM 5 LIVE). The video is played back at 6 frames/s. See Fig. 4.

Video 10. **High-magnification view of GFP-IFT20 dynamics in a control axoneme.** A single axoneme from Video 1 is shown. GFP-IFT43 particles move both antero- and retrogradely. Time-lapse images were acquired at 561-ms intervals for a total of 10.674 s by high-speed confocal microscopy on a microscope (LSM 5 LIVE). The video is played back at 6 frames/s. See Fig. 4.